J Coast Conserv (2016) 20:271–279
DOI 10.1007/s11852-016-0437-9

Estimating soil salinity in different landscapes of the Yellow River Delta through Landsat OLI/TIRS and ETM+ Data

Ling Meng[1,2] · **Shiwei Zhou**[3] · **Hua Zhang**[4] · **Xiaoli Bi**[4]

Received: 20 July 2015 / Revised: 15 April 2016 / Accepted: 16 April 2016 / Published online: 2 May 2016

Abstract Soil salinization has increasingly become a serious issue in coastal zone due to global climate changes and human disturbances. Assessment of soil salinity, especially at the landscape scale, is critical to coastal management and restoration. Two data from OLI/TIRS and ETM+ sensors of Landsat satellite were used to compare their ability to invert the spatial pattern of soil salinity in both farmland and salt marsh landscapes in the Yellow River Delta, China, respectively. The results showed that the in situ electrical conductivity (EC_a) of soil, representing soil salinity, were closely related with spectral parameters and salinity indices calculated by the remote sensing data. The results of multiple regression models have showed that nearly all the spectral parameters and salinity indices calculated by OLI/TRIS data were more sensitive to soil salinity than those by ETM+ data. Therefore, the models based on OLI/TIRS data are superior to those on ETM+ data in estimating the spatial pattern of soil salinity in farmland and salt marsh landscapes. Our results were very helpful to evaluate the levels of soil salinization in the Yellow River Delta.

Keywords Soil salinity · Electrical conductivity · Landsat OLI/TIRS · Landsat ETM+ · the Yellow River Delta

✉ Xiaoli Bi
xlbi@yic.ac.cn

[1] State Key Laboratory of Soil and Sustainable Agriculture, Institute of Soil Science, Chinese Academy of Sciences, Nanjing 210008, People's Republic of China

[2] Key Laboratory of Marine Environment and Ecology, Ministry of Education of China, Ocean University of China, Qingdao 266100, People's Republic of China

[3] Institute of Agricultural Resources and Regional Planning, Chinese Academy of Agricultural Sciences, Beijing 100081, People's Republic of China

[4] Key Laboratory of Coastal Environmental Processes and Ecological Remediation, Yantai Institute of Coastal Zone Research, Chinese Academy of Sciences, Yantai 264003, People's Republic of China

Introduction

Soil salinization is a form of soil degradation due to the buildup of solute salts to deleterious levels at or near the surface of the soil (Schofield et al. 2001). Solute salt accumulation is a complex and dynamic process affected by natural (e.g. climate, hydrology, topography, and geology) and human-induced (e.g. land use, irrigation) factors (Zhou et al. 2012). It is estimated that the worldwide salt-affected areas are close to 932 million ha, with more than 76 million ha as a consequence of human activities (Abrol et al. 1988; Mensah and FitzGibbon 2013).

Remote sensing technology has a great advantage over the traditional field investigation in monitoring soil salinity, particularly at the large areas due to its large coverage area, multiple spectra information and constant observation (Ding and Yu 2014). Numerous remote sensing data have been used to quantify the soil salinization, including the multispectral data acquired from the satellite-borne sensors (e.g., Landsat and SPOT series, Terra-ASTER, IRS-LISS, IKONIS, MODIS) (Dwivedi et al. 2008; Schmid et al. 2008; Abbas et al. 2013; Nawar et al. 2015), as well as hyperspectral data obtained from the airborne sensors (e.g. AVIRIS, HyMap, EO-1) (Farifteh et al. 2007; Weng et al. 2008; Whiting and Ustin 1999). The multispectral images, especially of the Landsat Thematic Mapper sensors (TM) or Enhanced Thematic Mapper Plus (ETM+) which are carried on-board the Landsat series have been widely used. A large number of studies have proved Landsat TM/ETM+ as a useful tool in monitoring soil surface

salinity (see. Sharma and Bhargava 1988; Metternicht and Zinck 1997; Fernandez-Buces et al. 2006; Howari and Goodell 2008; Wu et al. 2008; Arnous and Green 2015a).

In 2013, the Operational Land Imager (OLI) and Thermal Infrared Sensor (TIRS) sensors were launched on-board of Landsat-8, providing data consistent with previous Landsat series (in terms of acquisition geometry, coverage characteristics, and spectral characteristics) to make comparison for global and regional changes (Irons et al. 2012). Meanwhile, there are some differences: (1) OLI/TIRS uses long and linear arrays of detectors aligned across the instrument focal planes to collect imagery in a "push broom" manner, which improves the signal-to-noise performance compared to traditional "whiskbroom" sensor carried by the Landsat-5/7. The signal-to-noise of OLI/TIRS is three times higher than that of ETM+ data. The geometric stability and excellent image quality of the OLI/TIRS data were also improved by this "push broom" design (Irons et al. 2012) (Fig. 1.). (2) The OLI/TIRS also provide specific bandwidths besides the ETM+ shortwave bands (Xu and Tang 2013). However, little is known about the application of OLI/TIRS data on the mapping of soil salinization.

The Yellow River Delta (YRD) is a typical coastal delta characterized by extensive soil salinization. It was reported that 2.35×10^5 hm^2 of the region have been salinized in 2000 (Liu et al. 2003), since then, the salinization process has been accelerated because of the reduction of the Yellow River discharge, seawater intrusion, frequent storm surges, and coastal erosion (Zinck and Metternicht 2008). Mapping and monitoring the spatial distribution and temporal behavior of salt-affected soils in the YRD, therefore, is necessary to coastal management and soil restoration.

A natural salt marsh landscape in the Dawenliu Nature Reserve (DNR) and a farm landscape along the Yellow river (YRF) were selected to compare the capability of ETM+ and OLI/TIRS data to map soil salinity. Our main objectives were: (1) to assess the ability of OLI/TIRS data to predict soil salinity, compared with ETM+ data; (2) to develop a multi-regression model for characterizing soil salinity using OLI/TIRS data; and then (3) to realize the spatial mapping of the soil salinization in the YRD.

Study area

The YRD is located at the northeast coast of the Shandong Province, China (118°06′E-119°18′E, 36°55′N-38°16′N) and at the southern coast of the Bohai Sea (Qin et al. 2015), with an area of 6650 km^2. The YRD is one of the most active regions of land-ocean interaction among the large river deltas in the world where massive deposition of silt created a fast-growing natural delta before 1986 (Zhang and Hu 2007). The growth of the YRD is mainly affected by water discharge and suspended sediment load of Yellow River and subsequent changes of river channel (Li et al. 2009). However, the progradation process decreased and the coastal erosion increased due to the reduced sediment discharge in last three decades (Chu et al. 2006).

The area has temperate continental monsoon climate with distinctive seasons (Cui et al. 2009a). The average annual temperature here is around 11.7–12.6 °C, average annual potential evaporation is about 1900–2400 mm and annual precipitation is 530–630 mm (in which 70% amasses in summer) (Ye et al. 2004; Fang et al. 2005). The area of perennial waterlogged wetlands is 964.8 km^2, accounting for 63.06% of total area of the Yellow River Delta. Every year, approximately 1.05×10^7 tons of sand and soil are carried by the river from upstream and deposited in the delta, resulting in vast area of floodplain and special wetland landscape (Xu et al. 2002; Wang et al. 2004; Cui et al. 2009a).

There are completely different vegetation landscapes in the two study areas. The DNR, near the mouth of the Yellow River, has an area of 54, 962 ha and is established to protect coastal wetlands (Cui et al. 2009b). The area is dominated by the salt marsh species, such as the *Suaeda salsa, Tamarix chinensis, Phragmites australis* and *Imperata cylindrical*. The YRF,

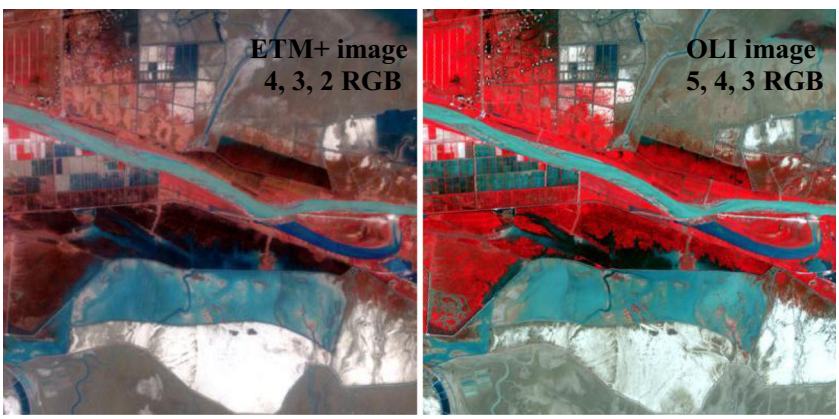

Fig. 1 Standard false color images of OLI and ETM+ sensors

southeast to Yellow River has an area of 45, 000 ha and is characterized by farmland of cotton and corn (Fig. 2.).

Materials and methods

Remote sensing data

ETM+ data (May 6, 2013) and OLI/TIRS data (May 30, 2013) were obtained from the U.S. Geological Survey (USGS) website (http://glovis.usgs.gov/). First, bad lines due to the Scan Lines Corrector (SLC) trouble of the ETM+ sensor were removed using the kriging geo-statistical technique (Zhang et al. 2007). Then the images were geo-referenced and geometrically rectified based on a 1:100, 000 topographic map of the study area (WGS 84 datum, UTM N 50 projection). An improved image-based dark object subtraction model was used to implement radiometric and atmospheric correction (Chavez 1996; Lu et al. 2007). All the remote sensing data was processed by the ENVI 4.7 software and the results were visualized by ArcGIS 9.3 software.

In addition to original bands of ETM+ and OLI/TIRS, four salinity indices (Table 1) were used to quantify the capability of the remote sensing data to characterize soil salinity. For instance, Salinity Index (SI) and Bright Index (BI) measured the surface brightness of soils with high salinity (Khan et al. 2005). Combined spectral response index (COSRI) is a combined spectral-response index derived from ETM+ which is significantly correlated with soil electrical conductivity (EC_a) (Fernandez-Buces et al. 2006). Normalized Difference Salinity Index (NDSI) is used to test relationship between vegetation and soil salinity (Khan et al. 2005).

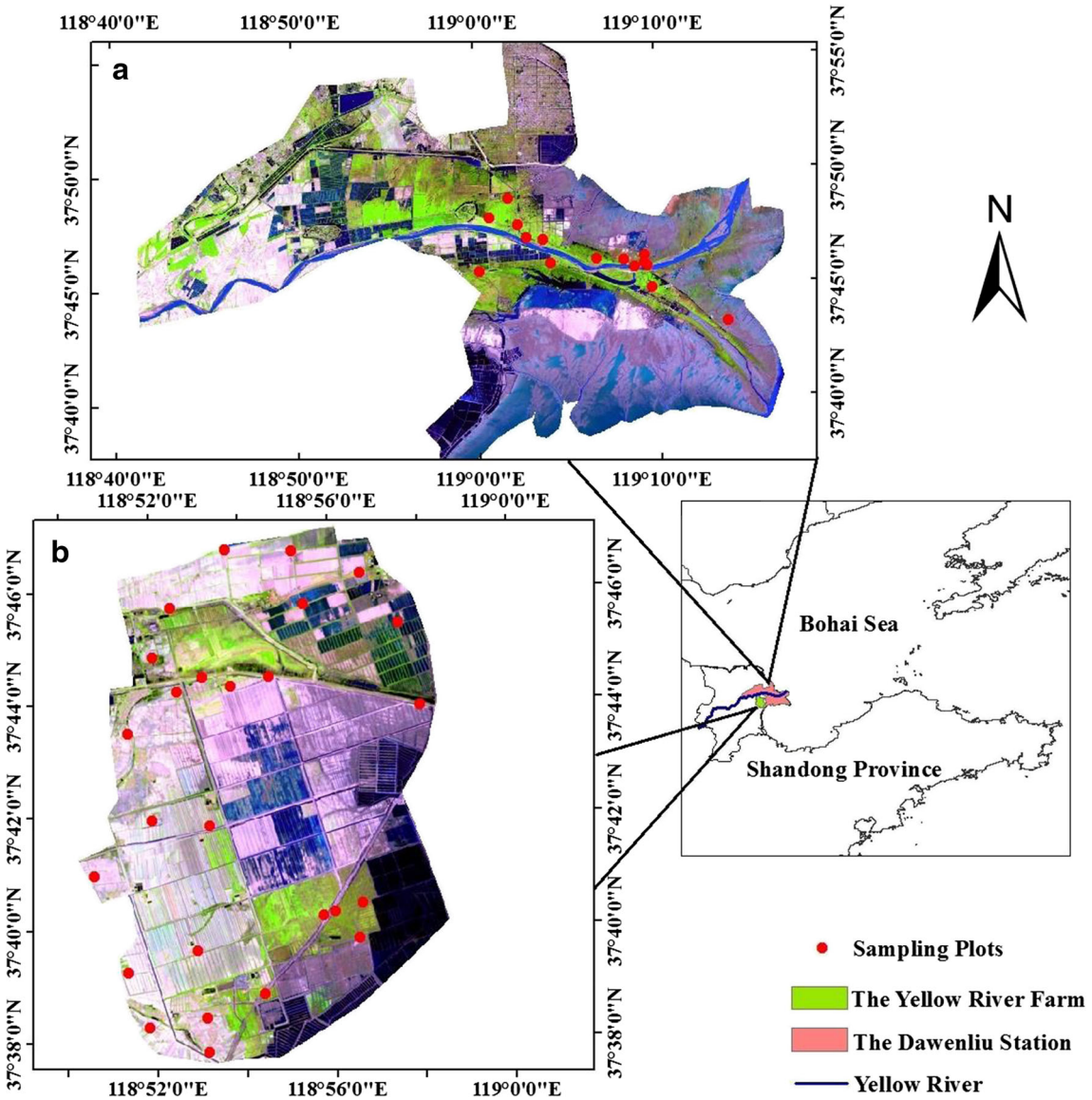

Fig. 2 Location of the study area: **a**. the Dawenliu Natural Reserve; and **b**. the Yellow River Farm

Table 1 Salinity indices and spectral functions

Salinity indices	Spectral Functions	References
Salinity Index (SI)	$\sqrt{band1 \times band3}$	(Khan et al. 2005)
Normalized Differential Salinity Index (NDSI)	$(band3 - band4)/(band3 + band4)$	(Khan et al. 2005)
Bright Index (BI)	$\sqrt{(band3)^2 + (band4)^2}$	(Khan et al. 2005)
Combined Spectral Response Index (COSRI)	$((band1 + band2)/(band3 + band4)) \times NDVI$	(Fernandez-Buces et al. 2006)

Plot investigation and EC_a measurement

42 plots in different vegetation types (15 in the DNR and 27 in the YRF) were chosen in April, 2013 (Fig. 2). For each plot, 4 points in orthogonal grid (500 × 500 m) were designed. Overall, there were 60 points in the DNR and 108 points in the YRF, respectively. EC_a was measured with the EM38 reader (Geonics), horizontal to the soil surface which had the high interpretation precision of the surface soil electrical conductivity (Yao et al. 2008). The coordinates of each point were recorded using a Global Positioning system (GPS, Garmin eTrex).

Statistical models and validation

Pearson correlation analysis was conducted between EC_a and spectral indices derived from ETM+ (7 original bands and 4 indices) and OLI/TIRS (10 original bands and 4 indices), respectively (Table 2). Multi-linear regression model was conducted to estimate soil EC_a from ETM+ and OLI/TIRS indices, with stepwise forward estimation method. EC_a data were randomly divided into two groups: 80% of those were used for constructing the multi-linear regression model and the other 20% for model validation. All statistical analysis was performed using the SPSS 16.0 software (SPSS Inc. 2010).

Results

Correlation between EC_a with spectrum information and salinity indices

Results of correlation analysis between EC_a and remote sensing data were shown in Table 2. For the ETM+ data, EC_a was significantly correlated with all spectral indices in YRF, and the whole study area (Overall). While in the DNR, besides the band1, band 2 and SI, other indices also matched well with EC_a.

For the OLI/TIRS data, four salinity indices were strongly correlated with EC_a. Nearly all bands were insignificantly related to EC_a in the whole study area except the NIR (band 5) and SWIR (band6, band7). In YRF and DNR, almost all of spectral bands were strongly

Table 2 Correlation coefficient (R) between measured soil electronic conductivity (EC_a) and individual spectral bands of Landsat 7 ETM+ and 8 OLI/TRIS for overall, the Yellow River Farm (YRF), and the Dawenliu Natural Reserve (DNR) datasets

Landsat 8 OLI/TRIS				Landsat 7 ETM+			
	Overall	YRF	DNR		Overall	YRF	DNR
Band 1	−0.12	−0.23*	−0.78**				
Band 2	−0.14	−0.32*	−0.77**	Band 1	−0.28*	−0.26*	−0.28
Band 3	−0.21*	−0.38**	−0.67**	Band 2	−0.34**	−0.38**	−0.23
Band 4	−0.14	−0.37**	−0.79**	Band 3	−0.33**	−0.41**	−0.05*
Band 5	−0.61**	−0.53**	−0.79**	Band 4	−0.65**	−0.62**	−0.75**
Band 6	−0.27**	−0.32*	0.02	Band 5	−0.63**	−0.64**	−0.59**
Band 7	−0.21*	−0.32*	−0.56**	Band 7	−0.53**	−0.57**	−0.46**
Band 9	0.04	0.01	0.08				
Band 10	−0.21	−0.34*	0.14	Band 6	−0.23*	−0.56**	−0.02
Band 11	−0.23*	−0.37**	0.17				
SI	−0.14	−0.35**	−0.79**	SI	−0.31**	−0.36**	−0.13
NDSI	0.30*	0.13	0.86**	NDSI	0.39**	0.30*	0.79**
BI	−0.56**	−0.51**	−0.70**	BI	−0.47**	−0.51**	−0.51**
COSRI	−0.26**	−0.05	−0.89**	COSRI	−0.47**	−0.41**	−0.81**

*$P < 0.05$; **$P < 0.01$

correlated with EC_a except some SWIR (band 6 and band 9) and TIR (band 10 and band 11). Above all, COSRI had the highest correlation with salinity of coastal marsh in DNR ($R=-0.89$), while BI was closely related to EC_a in YRM ($R=-0.51$).

Regression models

For the whole study area (Overall), the SWIR (band 7), the COSRI and the NDSI of ETM+ image were selected in the predict model with the R^2 value of 0.682 (Eq. 1), and the SWIR (band 5) of OLI/TIRS data was selected in the model with R^2 of 0.351 (Eq. 2). The Multi-linear regression model based on OLI/TIRS image had lower prediction ability than that on ETM+ data.

$$\begin{aligned} Predicted\ soil\ salinity = {} & -3.946band7 - 15712.014COSRI \\ & -15152.893band6 \\ & + 351.784\left(R^2 = 0.682, P = 0.0364\right) \end{aligned} \quad (1)$$

$$\begin{aligned} Predicted\ soil\ salinity = {} & -0.041band5 \\ & + 953.283\ \left(R^2 = 0.351, P = 0.001\right) \end{aligned} \quad (2)$$

However, in the YRF, the SWIR (band 5), TIR (band 6) and COSRI of ETM+ image were selected in the model with R^2 of 0.648 (Eq. 3). For OLI/TIRS image, the NIR (band 5), SWIR (band 6), blue (band 1, band 2) and COSIR were selected with R^2 of 0.656 (Eq. 4). OLI/TIRS based model would result in slightly better prediction to soil salinity than ETM+ based model.

$$\begin{aligned} Predicted\ soil\ salinity = {} & -8.281band5 - 1868.624COSRI \\ & -13.574band6 \\ & + 2609.880\ \left(R^2 = 0.648, P = 0.001\right) \end{aligned} \quad (3)$$

$$\begin{aligned} Predicted\ soil\ salinity = {} & -0.129band5 + 1186.969COSRI \\ & + 0.066band6 + 1.290band1 - 1.005band2 \\ & -2739.350\left(R^2 = 0.656, P = 0.001\right) \end{aligned} \quad (4)$$

In the DNR, for ETM+ image, the COSRI, NDSI and the TIR band (band 6) were selected (Eq. 5). While for OLI/TRIS image, the COSIR, NDSI, the TIR bands (band 10, band11), green (band 3) and dark blue (band 1) were selected (Eq. 6). Both the two models had high predictions of EC_a (with the $R^2=0.944$ for OLI/TRIS, $R^2=0.819$ for ETM+, respectively).

$$\begin{aligned} Predicted\ soil\ salinity = {} & -28707.924COSRI - 29271.124NDSI \\ & + 14.089band6 \\ & -1901.499\left(R^2 = 0.819, P = 0.013\right) \end{aligned} \quad (5)$$

$$\begin{aligned} Predicted\ soil\ salinity = {} & -8728.336COSRI - 3835.755NDSI \\ & -0.277band3 + 0.654band11 \\ & -0.436band10 + 0.381band1 \\ & -5745.807\left(R^2 = 0.944, P = 0.001\right) \end{aligned} \quad (6)$$

Model validation

Predicted soil EC was computed using OLI/TIRS data based on the Eqs. (4) and (6). EC_a versus predicted EC were plotted in Fig. 3, indicating that there was a high consistency between predicted and measured values in both the YRF($R^2=0.65$) and the DNR($R^2=0.82$). The prediction accuracy of the models based on OLI/TIRS image could meet our need of retrieving different salt classes, despite of underestimation of EC_a outcome.

Discussion

Soil reflectance from a remote sensing platform is often the mixed results of surface components such as: mineralogy, organic matter content, moisture content, particle size, iron oxide content, and surface conditions (Farifteh et al. 2006). Therefore, correlation analysis between spectral variables and electrical conductivity should consider the characteristics of soil surface.

The YRF is generally covered by bare soil with low moisture content. The main factors affecting the reflectance of bare soil are the mineralogy of salts, color and roughness of soils (Metternicht and Zinck 2003). The soil in this delta is rich in sodium, calcium, chlorides and sulphates (Weng and Gong 2006). In our case, the NIR and SWIR of ETM+ were strongly correlated with EC_a, which is consistent with Farifteh's work. He found the potentially useful spectral bands in the NIR and SWIR regions of TM data for salinity discrimination using the 2-D correlograms analysis (Farifteh et al. 2007). Band 6's performance could be attributed to the high content of soil carbonates in this area. Metternicht and Zinck (1997) found that salt-affected lands had high spectral reflectance, particularly in the blue and red range of the spectrum. However, the visible spectra (band 1–3) were found to have negative and low correlation in our analysis, probably due to the large coverage of low-saline soil.

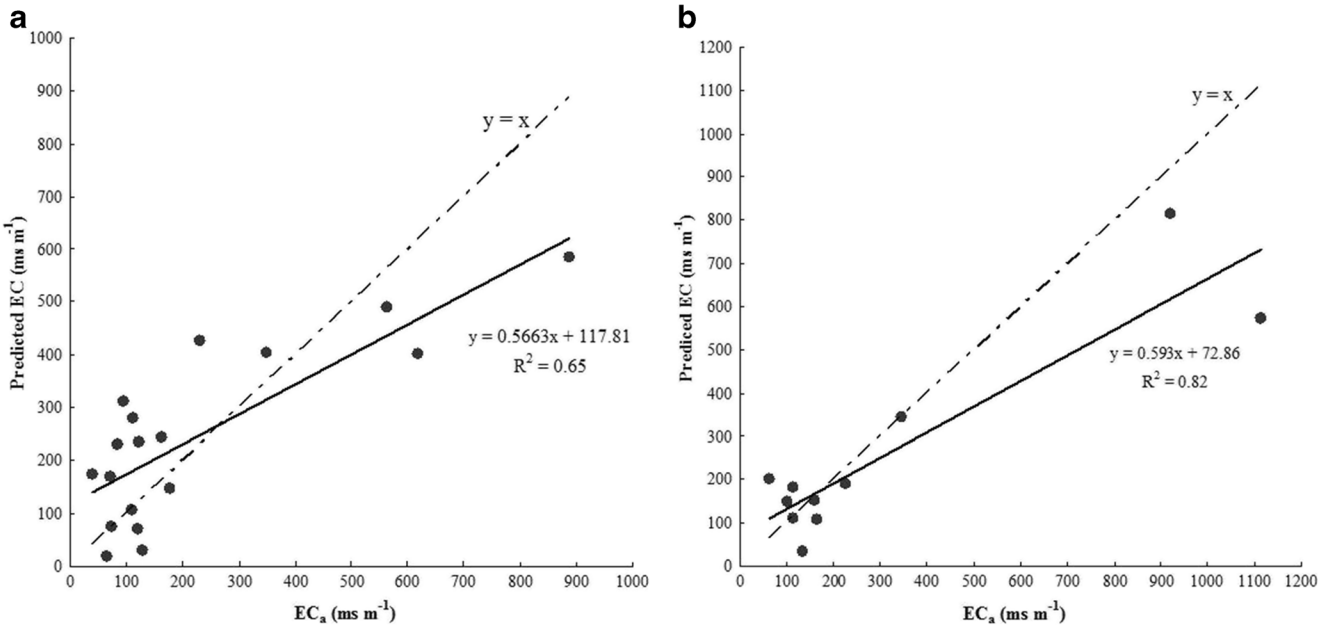

Fig. 3 Comparison between model predicted *EC* and measured apparent electronic conductivity (EC_a) at: **a** the Yellow River Farm; and **b** the Dawenliu Natural Reserve

Salt soils were often characterized by salt efflorescence accumulated on soil surface, so the salinity index BI which measured brightness from the soil surface was found to have significant relationship with soil salinity. Both NDSI and COSIR were not reliable indicators in the YRF considering the inhibitory effect of salt on the vegetation. The insignificant correlation of SI was in agreement with Setia's research. He has attributed the apparent lack of relationship of SI to the fragmented agriculture landscape (Setia et al. 2013). The OLI is required to collect data for all of the ETM+ shortwave bands to partially fulfill the data continuity mandate (Irons et al. 2012) and the spectral wavelength of OLI/TRIS in visible (band 2–5), NIR (band 4), SWIR (band 6, band 7) and thermal spectral (band 10, band11) is very similar to that of the ETM+, so the correlation between OLI bands and EC_a should be consistent with the ETM+ theoretically, but, in our research, the OLI/TIRS had been found poorly correlation with soil salinity. Surface condition, soil properties and environmental conditions could distribute the spectral signatures of salinity (Ben-Dor et al. 2009; Setia et al. 2013), thus, the factor influencing soil reflectance might be attributed to the change in environmental condition of the YRF. For instance, there was a large amount of precipitation during May 26–29, 2013, resulting in a lower correlation between visible bands (ETM+ band 1 (0.06), band 2 (0.00), band 3 (−0.04)) and NIR (band 4 (−0.10)), and a higher one for SWIR (ETM+ band 5 (−0.32), band 7 (−0.25)). This hypothesis could be proved by the measurements of reflected shortwave radiation (400–2500 nm) under changing moisture condition. Lobell and Asner have founded the absorption ability went up with the increase of wavelength from the visible bands, NIR to the SWIR (Lobell and Asner 2002).

The DNR was covered by halophytic plants which were all dry in our investigation. The vegetation coverage decreased with the increase of soil salinity. For ETM+ data, the vegetation-sensitive wavelength, i.e., NIR (band4), SWIR (band 5, band 7) and NDSI had relatively high correlation coefficient. COSRI was found to have the highest correlation with EC_a, which was in agreement with the other researches in the former lake Texcoco, Mexico, where the surface feature was similar to that of the DNR (Fernandez-Buces et al. 2006). The negative and low correlation of visible band and SI could be explained by the similar spectral reflection characteristic of the vegetation in the dry season. For OLI/TIRS data, nearly all variables except the thermal bands derived from the Landsat-8 had high correlation coefficient which was consistent with other results that it is also found the spectral bands of the OLI were sensitive to the salt-affected lands (Arnous et al. 2015b). But, the correlation coefficient from OLI/TIRS data was much higher than that obtained from the ETM+ data, which was in contrast with the results obtained in the YRF. We attributed the poor performance of OLI/TIRS data in the YRF to the increased soil moisture as mentioned above. However, OLI/TIRS's good performance in the DNR was contributed to the following reasons: (1) the surface of the DNR was generally covered with halophytic plants, meanwhile, the soil moisture was always in the supersaturated state here due to the high groundwater depth. Therefore, the precipitation could not influence the ground feature's reflectance; (2) since the OLI/TIRS data were obtained in growing season,

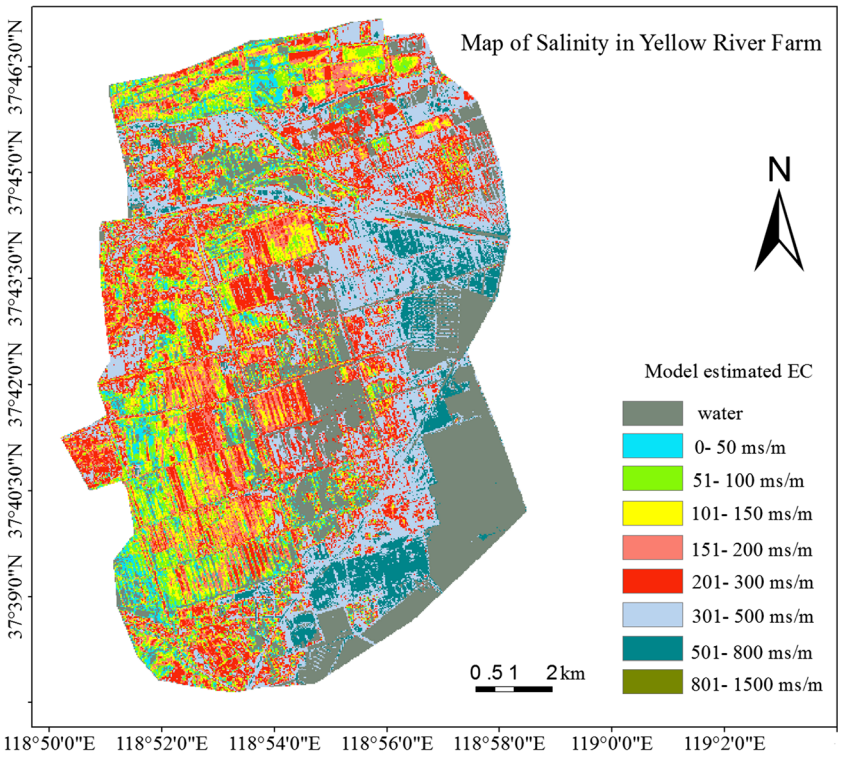

Fig. 4 Predicted *EC* of the Yellow River Farm. Values of predicted *EC* are calculated from Landsat OLI data using Eq. 4

it was mainly the reflection of the halophytic vegetation's spectral property. It was reported that halophytic plants (*S. salsa, T. chinensis* and *P. australis*) could reflectance peaks at the green and near- infrared band and absorption features at blue and red band, which had strong correlation with soil salinity (Zhang et al. 2012); (3) OLI/TIRS data has excellent image quality and high radiation resolution (Irons et al. 2012).

In the whole study area, however, our results showed that the model derived from the Landsat-8 data had poor ability to estimate soil salinity compared to the ETM+ data due to the interference of precipitation. When model suited to the YRF and the DNR, prediction accuracy resulted from the OLI/TIRS image was higher than those obtained from the ETM+ data, even if its accuracy reduced by the precipitation. Better radiation resolution and more detailed band wavelength set were certainly the main reasons for this difference. The results also indicated that the prediction models should consider the regional difference.

Mapping of salt soil had practical application for the two areas (Figs. 4 and 5). The degree of soil salinization was relatively weak in the YRF, with *EC* low than 300 *ms/m* for most of areas (Fig. 4). The spatial distribution was not obvious due

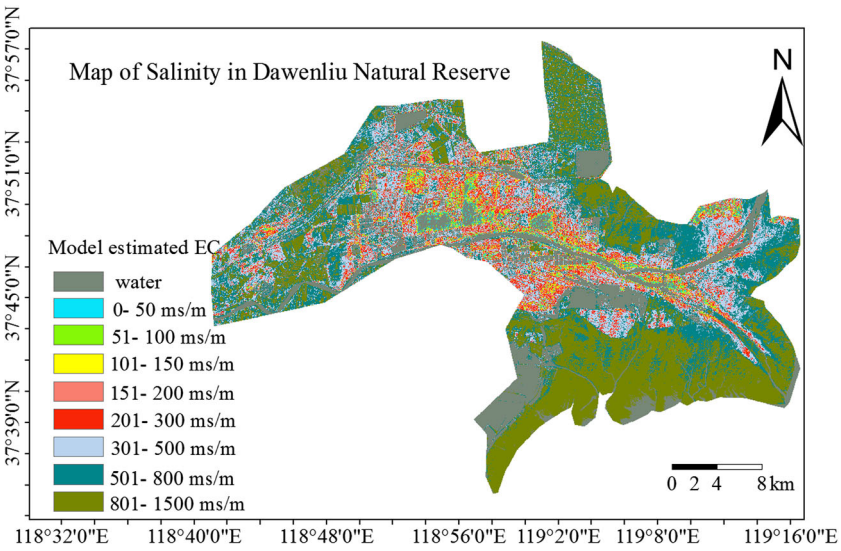

Fig. 5 Predicted *EC* of the Dawenliu Natural Reserve. Values of predicted *EC* are calculated from Landsat OLI data using Eq. 6

to the human intervention, with lower soil salinity near the Yellow River, reservoir and some canals and higher salinity near sea, which was attributed to the diluting effects of the fresh water obtained from the Yellow River, reservoir and some canals. However, the degree of the soil salinity was more severe in the DNR, with *EC* above 500 *ms/m* for more than 50% of areas (Fig. 5). And it has a regular pattern, exhibiting a significant increasing trend from the inland to shore, and also an increase far from the Yellow River, reservoir and some canals. This was mainly due to seawater intrusion and extreme tidal surges, as well as diluting effects of the fresh water to some extent. According to our work, the spatial assessment of soil salinity condition in the Yellow River Delta can help local soil manager to make practical measurement for soil conservation.

Conclusions

The capability of OLI/TRIS data (Landsat-8) and ETM+ data (Landsat-7) for inverting soil salinity in a coastal marsh (DNR) and irrigated farm land (YRF) in the Yellow River Delta, China was compared through analyzing the relationship between their band characters with soil electrical conductivity (EC_a). Statistical models indicated that OLI/TIRS and ETM+ spectral bands and derived indices have significantly negative correlation with soil EC_a. There was a significant difference in soil salinization between the two sites because of the different land cover types. Regression model based on OLI/TIRS data had higher accuracy in predicting soil salinization of these two different sites, with the coefficient of determination (R^2) of 0.656 in YRF and 0.944 in DNR, respectively. Our results had demonstrated that the Landsat OLI/TIRS had some advantage over the Landsat ETM+ for mapping and monitoring soil salinity. This work was helpful to soil management and soil restoration in coastal wetland.

Acknowledgments This research was funded by the State Key Laboratory of Soil and Sustainable Agriculture, Institute of Soil Science, Chinese Academy of Sciences (Grant No. KZZD-EW-14). The authors also thank the editor and the anonymous reviewers for their valuable comments and suggestions to improve this manuscript.

References

Abbas A, Khan S, Hussain N, Hanjra MA, Akbar S (2013) Characterizing soil salinity in irrigated agriculture using a remote sensing approach. Phys Chem Earth 55:43–52

Abrol IP, Yadav JSP, Massoud FI (1988) Salt-affected soils and their management. FAO Soils Bulletin 39, Food and Agriculture Organization of the United Nations, Rome

Arnous MO, Green DR (2015) Monitoring and assessing water-logged and salt-affected areas in the Eastern Nile Delta region, Egypt, using remotely sensed multi-temporal data and GIS. J Coast Res 19(3):369–391

Arnous MO, El-Rayes AE, Green DR (2015) Hydrosalinity and environmental land degradation assessment of the East Nile Delta region, Egypt. J Coast Res 19(4):491–513

Ben-Dor E, Chabrillat S, Dematte JAM, Taylor GR, Hill J, Whiting ML, Sommer S (2009) Using Imaging Spectroscopy to study soil properties. Remote Sens Environ 113:S38–S55

Chavez PS (1996) Image-based atmospheric corrections-revisited and improved. Photogramm Eng Remote Sens 62(9):1025–1035

Chu ZX, Sun XG, Zhai SK, Xu KH (2006) Changing pattern of accretion/erosion of the modern Yellow River (Huanghe) subaerial delta, China: Based on remote sensing images. Mar Geol 1(227):13–30

Cui BS, Yang QC, Yang ZF, Zhang KJ (2009a) Evaluating the ecological performance of wetland restoration in the Yellow River Delta, China. Ecol Eng 35(7):1090–1103

Cui BS, Tang N, Zhao XS, Bai JH (2009b) A management-oriented valuation method to determine ecological water requirement for wetlands in the Yellow River Delta of China. J Nat Conserv 17(3):129–141

Ding JL, Yu DL (2014) Monitoring and evaluating spatial variability of soil salinity in dry and wet seasons in the Werigan–Kuqa Oasis, China, using remote sensing and electromagnetic induction instruments. Geoderma 235:316–322

Dwivedi RS, Kothapalli RV, Singh AN, Metternicht G, Zinck J (2008) Generation of farm level information on salt-affected soils using IKONOS-II multispectral data. Remote Sensing of Soil Salinization: Impact on Land Management. CRC press, Taylor & Francis, Boca Raton 73–90

Fang HL, Liu GH, Kearney M (2005) Georelational analysis of soil type, soil salt content, landform, and land use in the Yellow River Delta, China. Environ Manag 35(1):72–83

Farifteh J, Farshad A, George RJ (2006) Assessing salt-affected soils using remote sensing, solute modelling, and geophysics. Geoderma 130(3):191–206

Farifteh J, Van der Meer FD, Atzberge C, Carranza EJM (2007) Quantitative analysis of salt-affected soil reflectance spectra: A comparison of two adaptive methods (PLSR and ANN). Remote Sens Environ 110(1):59–78

Fernandez-Buces N, Siebe C, Cram S, Palacio JL (2006) Mapping soil salinity using a combined spectral response index for bare soil and vegetation: A case study in the former lake Texcoco, Mexico. J Arid Environ 65(4):644–667

Howari FM, Goodell PC (2008) Characterization of salt-crust build-up and soil salinization in the United Arab Emirates by means of field and remote sensing techniques. Remote Sensing of Soil Salinization: Impact on Land Management. CRC press, Taylor & Francis, Boca Raton, 141–154

Irons JR, Dwyer JL, Barsi JA (2012) The next Landsat satellite: The Landsat Data Continuity Mission. Remote Sens Environ 122:11–21

Khan NM, Rastoskuev VV, Sato Y, Shiozawa S (2005) Assessment of hydrosaline land degradation by using a simple approach of remote sensing indicators. Agric Water Manag 77(1):96–109

Li SN, Wang GX, Deng W, Hu YM, Hu WW (2009) Influence of hydrology process on wetland landscape pattern: A case study in the Yellow River Delta. Ecol Eng 35(12):1719–1726

Liu GH, Ye QH, Liu QS (2003) The dynamic monitoring and digital simulation of ecological environment in Yellow River Delta. Science Press, Beijing

Lobell DB, Asner GP (2002) Moisture effects on soil reflectance. Soil Sci Soc Am J 66(3):722–727

Lu D, Batistella M, Mausel P, Moran E (2007) Mapping and monitoring land degradation risks in the Western Brazilian Amazon using multitemporal Landsat TM/ETM+ images. Land Degrad Dev 18(1):41–54

Mensah KO, FitzGibbon J (2013) Responsiveness of Ada Sea defence project to salt water intrusion associated with sea level rise. J Coast Res 17:75–84

Metternicht G, Zinck JA (1997) Spatial discrimination of salt-and sodium-affected soil surfaces. Int J Remote Sens 18(12):2571–2586

Metternicht GI, Zinck JA (2003) Remote sensing of soil salinity: potentials and constraints. Remote Sens Environ 85(1):1–20

Nawar S, Buddenbaum H, Hill J (2015) Digital mapping of soil properties using multivariate statistical analysis and ASTER data in an arid region. Remote Sens 2(7):1181–1205

Qin DH, Gao M, Wu XQ, Du XY, Bi XL (2015) Seasonal changes in soil TN and SOC in a seawall-reclaimed marsh in the Yellow River Delta, China. J Coast Res 19(1):79–84

Schmid T, Koch M, Gumuzzio J (2008) Applications of hyperspectral imagery to soil salinity mapping. Remote Sensing of Soil Salinization: Impact on Land Management. CRC press, Taylor & Francis, Boca Raton, 113–140

Schofield R, Thomas D, Kirkby MJ (2001) Causal processes of soil salinization in Tunisia, Spain and Hungary. Land Degrad Dev 12(2):163–181

Setia R, Lewis M, Marschner P, Raja Segaran R, Summers D, Chittleborough D (2013) Severity of salinity accurately detected and classified on a paddock scale with high resolution multispectral satellite imagery. Land Degrad Dev 24(4):375–384

Sharma RC, Bhargava GP (1988) Landsat imagery for mapping saline soils and wet lands in north-west India. J Remote Sens 9(1):39–44

Wang FY, Liu RJ, Lin XG, Zhou JM (2004) Arbuscular mycorrhizal status of wild plants in saline–alkaline soils of the Yellow River Delta. Mycorrhiza 14:133–137

Weng YL, Gong P (2006) Soil salinity measurements on the Yellow River Delta. J Nanjing Univ (Nat Sci Edit) 42(6):602–610

Weng YL, Gong P, Zhu ZL (2008) Reflectance spectroscopy for the assessment of soil salt content in soils of the Yellow River Delta of China. Int J Remote Sens 29(19):5511–5531

Whiting ML, Ustin SL (1999) Use of low altitude AVIRIS data for identifying salt affected soil surfaces in Western Fresno County, California. University of California [http://www.cstars.ucdavis.edu/papers/html/whitingetal1999a/paperfr.html]

Wu JW, Vincent B, Yang JZ, Bouarfa S, Vidal A (2008) Remote sensing monitoring of changes in soil Salinity: A case study in Inner Mongolia, China. Sensors 8(11):7035–7049

Xu HQ, Tang F (2013) Analysis of new characteristics of the first Landsat 8 image and their ecoenvironmental significance. Acta Ecol Sin 33(11):3249–3257

Xu XG, Guo HH, Chen XL, Lin HP, Du QI (2002) A multi-scale study on land use and land cover quality change: the case of the Yellow River Delta in China. GeoJournal 56(3):177–183

Yao RJ, Yang J, Liu GM (2008) Application of electromagnetic induction EM38 to rapid analysis of soil salinization in the Yellow River Delta. Agric Res Arid Area 26(1):67–73

Ye QH, Tian GL, Liu GH, Ye JM, Yao X, Liu QS, Lou WG, Wu SG (2004) Tupu methods of spatial-temporal pattern on land use change: a case study in the Yellow River Delta. J Geogr Sci 14(2):131–142

Zhang ZH, Hu CH (2007) Variation of the processes of flow and sediment and its effect on epeirogenesis of seacoast in the Yellow River estuary. Adv Water Sci 18(3):336

Zhang C, Li W, Travis D (2007) Gaps-fill of SLC-off Landsat ETM+ satellite image using a geostatistical approach. Int J Remote Sens 22(28):5103–5122

Zhang F, Tashpolat T, Ding JL, Mamat S, Gui DW (2012) Spectral reflectance characteristics of typical halophytes in the oasis salinization-desert zone on middle reaches of Tarim River, China. Chi J Plant Ecol 36(7):607–617

Zhou D, Lin ZL, Liu LM (2012) Regional land salinization assessment and simulation through cellular automaton-Markov modeling and spatial pattern analysis. Sci Total Environ 439: 260–274

Zinck JA, Metternicht G (2008) Soil salinity and salinization hazard. Remote Sensing of Soil Salinization: Impact on Land Management. CRC press, Taylor & Francis, Boca Raton, 3–20